An Energy-Preserving MAC–Yee Scheme for the Incompressible MHD Equation

Jian-Guo Liu* and Wei-Cheng Wang†

Institute for Physical Science and Technology and Department of Mathematics, University of Maryland, College Park, Maryland 20742; and †Department of Mathematics, National Tsing Hua University, Hsinchu, Taiwan
E-mail: jliu@math.umd.edu, wangwc@math.nthu.edu.tw

We propose a simple and efficient finite-difference method for the incompressible MHD equation. The numerical method combines the advantage of the MAC scheme for the Navier–Stokes equation and Yee's scheme for the Maxwell equation. In particular, the semi-discrete version of our scheme introduces no numerical dissipation and preserves the energy identity exactly.   © 2001 Elsevier Science

Key Words: incompressible MHD equation; finite-difference method; MAC scheme; Yee scheme; energy preserving.

1. INTRODUCTION

We propose a finite-difference method for the unsteady incompressible magnetohydrodynamics (MHD) equation

$$\rho(\partial_t \boldsymbol{u} + \boldsymbol{u} \cdot \nabla \boldsymbol{u}) + \nabla p = \mu \Delta \boldsymbol{u} + \frac{1}{c} \boldsymbol{j} \times \boldsymbol{b}$$

$$\nabla \cdot \boldsymbol{u} = 0$$

$$\frac{1}{c} \partial_t \boldsymbol{b} + \nabla \times \boldsymbol{e} = \boldsymbol{0} \quad \text{in } \Omega \qquad (1.1)$$

$$\nabla \times \boldsymbol{b} = \frac{4\pi}{c} \boldsymbol{j}$$

$$\boldsymbol{j} = \sigma \left(\boldsymbol{e} + \frac{1}{c} \boldsymbol{u} \times \boldsymbol{b} \right),$$

with no-slip and perfectly conducting wall conditions

$$\boldsymbol{u} = \boldsymbol{0}, \quad \boldsymbol{e} \times \boldsymbol{\nu} = \boldsymbol{0} \quad \text{on } \Gamma = \partial\Omega, \qquad (1.2)$$

where ρ is the fluid density, $\boldsymbol{u}$ is the fluid velocity, and $\boldsymbol{b}$, $\boldsymbol{j}$, and $\boldsymbol{e}$ are the magnetic field, the electric current density, and the electric field, respectively. μ, σ, and c are physical

constants representing the viscosity coefficient, the electric conductivity, and the speed of light, respectively.

Equation (1.1) can be roughly divided into two parts: the Navier–Stokes equation governing the motion of the solenoidal fluid motion and the Faraday equation describing the evolution of the magnetic field. They are coupled together through the Lorentz force $\boldsymbol{j} \times \boldsymbol{b}$ and the electromotive force $\boldsymbol{u} \times \boldsymbol{b}$.

A major research topic on (1.1) is the regularity of the solution. For the viscous and resistive case ($\nu > 0, \sigma < \infty$), Duvaut and Lions [7] constructed a class of global-in-time weak solutions and local-in-time strong solutions similar to the Leray–Hopf weak solutions for the Navier–Stokes equation. Further partial regularity results can be found in [13, 14, 23]. Most of the results are similar to partial regularity results for the Navier–Stokes equation. In particular, the 2-D solution is shown to be smooth [23]. It is worth noting that the one-point-singular solution constructed in [26] for the Navier–Stokes equation does not have a counterpart in the MHD equation [14], suggesting some kind of regularization effect in the presence of the magnetic field.

To date, whether or not smooth initial data for the ideal MHD ($\mu = 0, \sigma = \infty$) would develop singularity in finite time remains open, even in the 2-D case. An MHD version of the Beale–Kato–Majda theorem in [4] gives a necessary condition for blowup of smooth solutions. Namely, if smooth initial data lead to a singularity at time T, then

$$\int_0^T \|\boldsymbol{\omega}(t)\|_{L^\infty} + \|\boldsymbol{j}(t)\|_{L^\infty} \, dt = \infty. \tag{1.3}$$

This suggests that $\|\boldsymbol{\omega}(t)\|_{L^\infty} + \|\boldsymbol{j}(t)\|_{L^\infty}$ is the only quantity that needs to be traced during numerical simulations in search of possible singularities.

In numerical experiments for ideal 2-D flows, strong current sheets are often observed. This singularity-like structure is a thin stretched region of high concentration of current density. Exponential growth rate in current density has been observed [6, 9, 22] for the current sheet associated with a hyperbolic saddle of the magnetic potential (also known as an X point in plasma literature). A scaling argument was proposed in [22] to account for the observed exponential growth rate. Partial regularity results concerning flow structure near an X point can be found in [6, 9]. It is worth mentioning that the scenario of blowup near an X point is excluded under mild assumptions of the velocity field [9]. However, the possibility of blowup outside an X point remains open. The 3-D flow structure is even more complicated and the conclusions of different numerical simulations seem controversial [10, 18].

The purpose of this paper is to propose a simple and efficient finite-difference method for (1.1) at large Reynolds number. Typical difficulties in the numerical computation of (1.1) are similar to those in computational fluid dynamics, such as enforcing the incompressibility constraint of velocity field, the realization of no-slip boundary condition, and in particular the resolution of the boundary layer and small-scale flows at large Reynolds number. In addition, in contrast to the explicit incompressibility constraint of the velocity field, the Faraday equation does not have a Lagrangian multiplier. The magnetic field is necessarily divergence free since the source term is a perfect curl. It is important that the numerical scheme keeps the magnetic field divergence free automatically. Failure to maintain the incompressibility constraint for the magnetic field is known to result in spurious numerical solutions [3]. In addition to accuracy consideration, efficiency is a major concern. The cost

of directly solving the coupled 3-D system (1.1) is enormous, especially in the presence of physical boundaries. To effectively decouple the system (1.1), we insist on treating the nonlinear terms *explicitly*. The viscous and resistive terms can be treated either explicitly or implicitly depending on the magnitude of the Reynolds number and the magnetic Reynolds number. With a proper choice of staggered grids, the boundary conditions (1.2) can be realized easily with a local formula. Therefore we effectively break the system into separate smaller systems that can be solved using the standard fast Poisson solvers. By using classical third- or fourth-order Runge–Kutta time discretization, the time stepping is determined by the CFL condition only without cell Reynolds number constraint [8]. Altogether, the resulting scheme is simple, robust, and efficient.

The most remarkable feature of our scheme is to treat the spatial discretization of the nonlinear term carefully with central differencing and proper averaging so that the resulting semi-discrete version of our scheme preserves the energy identity (3.9) and the divergence-free constraint for both velocity and magnetic field exactly. As a result, the scheme is nonlinearly stable and free from excess numerical viscosity. In addition, the cross-helicity identity (3.17) is also preserved numerically. This makes the scheme suitable for large time direct numerical simulation. In view of (1.3), the absence of excess numerical viscosity also helps to identify possible singularities. A preliminary test of our scheme on 2-D ideal MHD with strong current sheet gives satisfactory results; see Section 5 for details.

The rest of the paper is organized as follows: In Section 2, we describe the scheme in detail. We then derive the energy identity and its discrete analogue in as well as the cross-helicity identity, in Section 3. In Section 4, we discuss equivalent numerical formulations of our scheme and comment on their efficiency, and finally we present a few numerical test problems in Section 5.

2. THE MAC–YEE SCHEME

The scheme presented here combines two well-known methods in computational fluid dynamics and computational electromagnetic waves, namely, the MAC scheme and Yee's scheme. We use the MAC scheme to decouple the pressure Poisson equation from the momentum equation, keeping the velocity field divergence free. The Faraday equation, however, does not have a Lagrangian multiplier to perform the Hodge decomposition. With the setting introduced by Yee [28], we can evaluate the discrete curl of the magnetic field in a natural way and enforce the discrete divergence-free constraint automatically. In addition, we have carefully chosen the spatial discretization of the nonlinear terms in a way such that a discrete version of the energy identity is satisfied; see Theorem 1.

2.1. *Notations*

We start with the mesh description (see also Fig. 1): For simplicity in presentation, we assume that the physical domain is a cube divided into $N_1 \times N_2 \times N_3$ equally sized cubic cells. Defined on the center of each cell interface are the normal components of $\boldsymbol{u}$ and $\boldsymbol{b}$ representing the approximate mean flux across the interface. We use the notation "$\Rightarrow$," "$\Uparrow$," and "$\odot$", indexed by $(i, j - \frac{1}{2}, k - \frac{1}{2})$, $(i - \frac{1}{2}, j, k - \frac{1}{2})$, and $(i - \frac{1}{2}, j - \frac{1}{2}, k)$ to denote the interfaces perpendicular to x, y, and z directions, respectively. The tangential components of $\boldsymbol{j}$ and $\boldsymbol{\omega}$ are defined on the edge centers. Edges in the x, y, and z directions are labeled "$\rightarrow$," "$\uparrow$," and "$\odot$" with indices $(i - \frac{1}{2}, j, k)$, $(i, j - \frac{1}{2}, k)$, and $(i, j, k - \frac{1}{2})$,
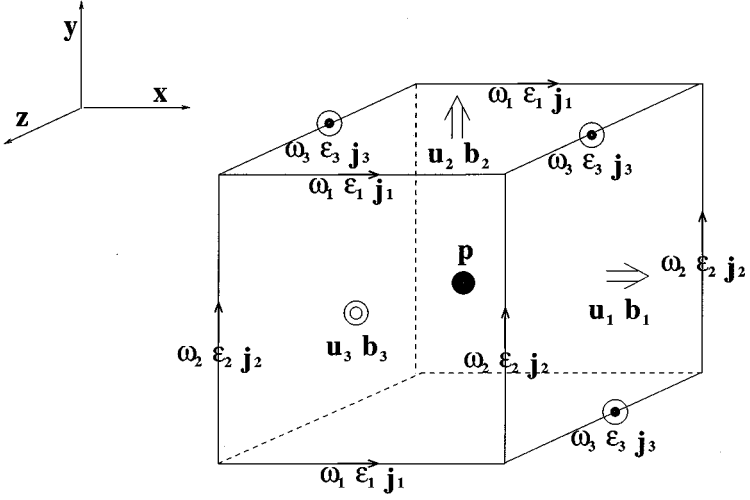
FIG. 1. Mesh depiction for the 3-D MAC–Yee scheme.

respectively. Finally the pressure is defined on the center of each cell, the "$\bullet$" points indexed by $(i - \frac{1}{2}, j - \frac{1}{2}, k - \frac{1}{2})$.

For convenience, we denote all the interior faces, edges, and cubes in Ω by

$$
\begin{aligned}
\Omega_F &= \{\text{"}\Rightarrow\text{", "}\Uparrow\text{", and "}\odot\text{"} \quad \text{in } \Omega\} \\
\Omega_E &= \{\text{"}\rightarrow\text{", "}\uparrow\text{", and "}\odot\text{"} \quad \text{in } \Omega\} \\
\Omega_C &= \{\text{"}\bullet\text{"}\},
\end{aligned}
\tag{2.1}
$$

the boundary faces and edges by

$$
\begin{aligned}
\Gamma_F &= \{\text{"}\Rightarrow\text{", "}\Uparrow\text{", and "}\odot\text{"} \quad \text{on } \Gamma\} \\
\Gamma_E &= \{\text{"}\rightarrow\text{", "}\uparrow\text{", and "}\odot\text{"} \quad \text{on } \Gamma\},
\end{aligned}
\tag{2.2}
$$

and

$$
\bar{\Omega}_F = \Omega_F \cup \Gamma_F, \qquad \bar{\Omega}_E = \Omega_E \cup \Gamma_E.
\tag{2.3}
$$

For convenience, we also denote

$$
\begin{aligned}
\bar{\bar{\Omega}}_F &= \bar{\Omega}_F \cup \{\text{ghost faces}\} \\
\bar{\bar{\Omega}}_E &= \bar{\Omega}_E \cup \{\text{ghost edges}\} \\
\bar{\bar{\Omega}}_C &= \Omega_C \cup \{\text{ghost centers}\}.
\end{aligned}
\tag{2.4}
$$

By a ghost point we mean a point half mesh size away from Ω. For example, the "ghost centers" will then be indexed by $(i - \frac{1}{2}, j - \frac{1}{2}, k - \frac{1}{2})$ with $(i = 0, N_1 + 1, j = 1, \ldots, N_2, k = 1, \ldots, N_3)$, $(i = 1, \ldots, N_1, j = 0, N_2 + 1, k = 1, \ldots, N_3)$, and $(i = 1, \ldots, N_1, j = 1, \ldots, N_2, k = 0, N_3 + 1)$.

We write $\boldsymbol{f} = (f_1, f_2, f_3)^T \in L^2(\Omega_F)$ (or $L^2(\bar{\Omega}_F)$, $L^2(\bar{\bar{\Omega}}_F)$) if

$$\boldsymbol{f} = \begin{cases} f_1 & \text{on "}\Rightarrow\text{"} \\ f_2 & \text{on "}\Uparrow\text{"} \\ f_3 & \text{on "}\odot\text{",} \end{cases} \tag{2.5}$$

with f_1, f_2, and f_3 square summable. $L^2(\Omega_E)$, $L^2(\Omega_C)$, $L^2(\Gamma_F)$, and $L^2(\Gamma_E)$ are similarly defined.

The differencing and averaging operators in the x direction are defined as

$$\mathcal{D}_1 f(x, y, z) = \frac{f(x + \Delta x/2, y, z) - f(x - \Delta x/2, y, z)}{\Delta x},$$

$$\mathcal{A}_1 f(x, y, z) = \frac{f(x + \Delta x/2, y, z) + f(x - \Delta x/2, y, z)}{2}.$$

$\mathcal{D}_2 f$, $\mathcal{D}_3 f$, $\mathcal{A}_2 f$, and $\mathcal{A}_3 f$ are defined in a similar way.

On a boundary face, we use

$$f_\nu = \boldsymbol{f} \cdot \boldsymbol{\nu} \tag{2.6}$$

to denote the component along the outward unit normal $\boldsymbol{\nu}$, whereas on a boundary edge, we denote by $\boldsymbol{\tau}$ the unit tangent vector along that edge,

$$\boldsymbol{\tau}' = \boldsymbol{\nu} \times \boldsymbol{\tau}, \tag{2.7}$$

and similarly define the tangential components

$$g_\tau = \boldsymbol{g} \cdot \boldsymbol{\tau}, \qquad g_{\tau'} = \boldsymbol{g} \cdot \boldsymbol{\tau}'. \tag{2.8}$$

On either a boundary face or a boundary edge, $\mathcal{A}_\nu$ denotes the averaging operator in the normal direction (over an interior point and a ghost point outside the physical domain) and $\mathcal{D}_\nu$ the differencing operator along the outward normal. For example, if Γ contains a portion of the plane $\{x = 0\}$ with $\{x > 0\}$ being the interior, we have

$$\mathcal{D}_\nu f(0, y, z) = \frac{f(-\Delta x/2, y, z) - f(\Delta x/2, y, z)}{\Delta x},$$

$$\mathcal{A}_\nu f(0, y, z) = \frac{f(-\Delta x/2, y, z) + f(\Delta x/2, y, z)}{2}.$$

For $\boldsymbol{f} \in L^2(\bar{\Omega}_F)$, $\boldsymbol{g} \in L^2(\bar{\Omega}_E)$, and $q \in L^2(\Omega_C)$, we define the discrete divergence, curl, and gradient operators as

$$\nabla_h \cdot \boldsymbol{f} = (\mathcal{D}_1 f_1 + \mathcal{D}_2 f_2 + \mathcal{D}_3 f_3) \quad \text{on } \Omega_C, \tag{2.9}$$

$$\nabla_h \times \boldsymbol{f} = (\mathcal{D}_2 f_3 - \mathcal{D}_3 f_2, \mathcal{D}_3 f_1 - \mathcal{D}_1 f_3, \mathcal{D}_1 f_2 - \mathcal{D}_2 f_1) \quad \text{on } \Omega_E, \tag{2.10}$$

$$\nabla_h \times \boldsymbol{g} = (\mathcal{D}_2 g_3 - \mathcal{D}_3 g_2, \mathcal{D}_3 g_1 - \mathcal{D}_1 g_3, \mathcal{D}_1 g_2 - \mathcal{D}_2 g_1) \quad \text{on } \bar{\Omega}_F, \tag{2.11}$$

and

$$\nabla_h q = (\mathcal{D}_1 q, \mathcal{D}_2 q, \mathcal{D}_3 q) \quad \text{on } \Omega_F. \tag{2.12}$$

Since $\mathcal{D}_i\mathcal{D}_j = \mathcal{D}_j\mathcal{D}_i$, it is obvious that

$$\nabla_h \times (\nabla_h q) = \mathbf{0}, \tag{2.13}$$

$$\nabla_h \cdot (\nabla_h \times \mathbf{g}) = 0, \tag{2.14}$$

and

$$\Delta_h f = \left(\mathcal{D}_1^2 + \mathcal{D}_2^2 + \mathcal{D}_3^2\right)f = -\nabla_h \times \nabla_h \times f + \nabla_h(\nabla_h \cdot f). \tag{2.15}$$

2.2. *The Semi-discrete Scheme*

To describe the MAC–Yee scheme, we first rewrite (1.1) in dimensionless form with the convection term $\mathbf{u} \cdot \nabla\mathbf{u}$ replaced by $\boldsymbol{\omega} \times \mathbf{u} + \nabla|\mathbf{u}|^2/2$. The new Lagrangian multiplier $p/\rho + |\mathbf{u}|^2/2$ is still denoted by p:

$$\partial_t \mathbf{u} + \boldsymbol{\omega} \times \mathbf{u} + \nabla p = -\nu\nabla \times \boldsymbol{\omega} + \alpha \mathbf{j} \times \mathbf{b} \tag{2.16}$$

$$\nabla \cdot \mathbf{u} = 0 \tag{2.17}$$

$$\partial_t \mathbf{b} - \nabla \times \varepsilon = -\eta\nabla \times \mathbf{j} \tag{2.18}$$

$$\boldsymbol{\omega} = \nabla \times \mathbf{u}, \quad \mathbf{j} = \nabla \times \mathbf{b}, \quad \varepsilon = \mathbf{u} \times \mathbf{b}. \tag{2.19}$$

The three free parameters ν^{-1}, η^{-1}, and $\alpha^{-1/2}$ are known as Reynolds number, magnetic Reynolds number, and Alfvén number.

The semi-discrete version of the energy-preserving MAC–Yee scheme is given by

$$\frac{d}{dt}u_1 + \mathcal{A}_3(\omega_2\mathcal{A}_1 u_3) - \mathcal{A}_2(\omega_3\mathcal{A}_1 u_2) + \mathcal{D}_1 p$$
$$= -\nu(\mathcal{D}_2\omega_3 - \mathcal{D}_3\omega_2) + \alpha(\mathcal{A}_3(j_2\mathcal{A}_1 b_3) - \mathcal{A}_2(j_3\mathcal{A}_1 b_2)) \quad \text{on "}\Rightarrow\text{"}$$

$$\frac{d}{dt}u_2 + \mathcal{A}_1(\omega_3\mathcal{A}_2 u_1) - \mathcal{A}_3(\omega_1\mathcal{A}_2 u_3) + \mathcal{D}_2 p$$
$$= -\nu(\mathcal{D}_3\omega_1 - \mathcal{D}_1\omega_3) + \alpha\,(\mathcal{A}_1(j_3\mathcal{A}_2 b_1) - \mathcal{A}_3(j_1\mathcal{A}_2 b_3)) \quad \text{on "}\Uparrow\text{"} \tag{2.20}$$

$$\frac{d}{dt}u_3 + \mathcal{A}_2(\omega_1\mathcal{A}_3 u_2) - \mathcal{A}_1(\omega_2\mathcal{A}_3 u_1) + \mathcal{D}_3 p$$
$$= -\nu(\mathcal{D}_1\omega_2 - \mathcal{D}_2\omega_1) + \alpha(\mathcal{A}_2(j_1\mathcal{A}_3 b_2) - \mathcal{A}_1(j_2\mathcal{A}_3 b_1)) \quad \text{on "}\odot\text{"}$$

$$\mathcal{D}_1 u_1 + \mathcal{D}_2 u_2 + \mathcal{D}_3 u_3 = 0 \quad \text{on "}\bullet\text{"} \tag{2.21}$$

$$\frac{d}{dt}b_1 - (\mathcal{D}_2\varepsilon_3 - \mathcal{D}_3\varepsilon_2) = -\eta(\mathcal{D}_2 j_3 - \mathcal{D}_3 j_2) \quad \text{on "}\Rightarrow\text{"}$$

$$\frac{d}{dt}b_2 - (\mathcal{D}_3\varepsilon_1 - \mathcal{D}_1\varepsilon_3) = -\eta(\mathcal{D}_3 j_1 - \mathcal{D}_1 j_3) \quad \text{on "}\Uparrow\text{"} \tag{2.22}$$

$$\frac{d}{dt}b_3 - (\mathcal{D}_1\varepsilon_2 - \mathcal{D}_2\varepsilon_1) = -\eta(\mathcal{D}_1 j_2 - \mathcal{D}_2 j_1) \quad \text{on "}\odot\text{"}$$

with

$$\omega_1 = \mathcal{D}_2 u_3 - \mathcal{D}_3 u_2, \quad j_1 = \mathcal{D}_2 b_3 - \mathcal{D}_3 b_2, \quad \varepsilon_1 = (\mathcal{A}_3 u_2)(\mathcal{A}_2 b_3) - (\mathcal{A}_2 u_3)(\mathcal{A}_3 b_2) \quad \text{on "}\rightarrow\text{"}$$

$$\omega_2 = \mathcal{D}_3 u_1 - \mathcal{D}_1 u_3, \quad j_2 = \mathcal{D}_3 b_1 - \mathcal{D}_1 b_3, \quad \varepsilon_2 = (\mathcal{A}_1 u_3)(\mathcal{A}_3 b_1) - (\mathcal{A}_3 u_1)(\mathcal{A}_1 b_3) \quad \text{on "}\uparrow\text{"}$$

$$\omega_3 = \mathcal{D}_1 u_2 - \mathcal{D}_2 u_1, \quad j_3 = \mathcal{D}_1 b_2 - \mathcal{D}_2 b_1, \quad \varepsilon_3 = (\mathcal{A}_2 u_1)(\mathcal{A}_1 b_2) - (\mathcal{A}_1 u_2)(\mathcal{A}_2 b_1) \quad \text{on "}\odot\text{."}$$
$$\tag{2.23}$$

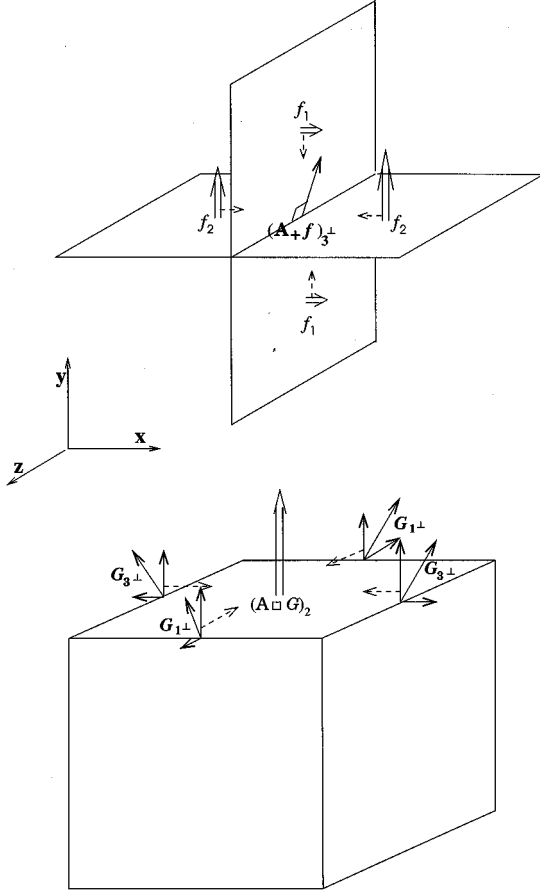**FIG. 2.** The two averaging operators $\mathcal{A}_+$ and $\mathcal{A}_\square$.

We simplify the expression for (2.20)–(2.23) as

$$\partial_t \boldsymbol{u} + \mathcal{A}_\square(\boldsymbol{\omega} \times \mathcal{A}_+ \boldsymbol{u}) + \nabla_h p = -\nu \nabla_h \times \boldsymbol{\omega} + \alpha \mathcal{A}_\square(\boldsymbol{j} \times \mathcal{A}_+ \boldsymbol{b}) \quad \text{on } \Omega_F \quad (2.24)$$

$$\nabla_h \cdot \boldsymbol{u} = 0 \quad \text{on } \Omega_C \quad (2.25)$$

$$\partial_t \boldsymbol{b} - \nabla_h \times \boldsymbol{\varepsilon} = -\eta \nabla_h \times \boldsymbol{j} \quad \text{on } \Omega_F \quad (2.26)$$

$$\boldsymbol{\omega} = \nabla_h \times \boldsymbol{u}, \quad \boldsymbol{j} = \nabla_h \times \boldsymbol{b}, \quad \boldsymbol{\varepsilon} = \mathcal{A}_+ \boldsymbol{u} \times \mathcal{A}_+ \boldsymbol{b}, \quad \text{on } \Omega_E \quad (2.27)$$

by introducing two averaging operators $\mathcal{A}_+$ and $\mathcal{A}_\square$ (see Fig. 2): $\mathcal{A}_+$ takes vectors on four adjacent faces onto the center of their common edge, resulting in a vector field defined on the edge centers with value transversal to the edge, denoted by $L^2(\bar{\Omega}_E; E^\perp)$,

$$\mathcal{A}_+ : L^2(\bar{\bar{\Omega}}_F) \mapsto L^2(\bar{\Omega}_E; E^\perp)$$

$$\mathcal{A}_+ \boldsymbol{f} = \boldsymbol{G} = \begin{cases} \boldsymbol{G_{1^\perp}} = (0, (G_{1^\perp})_2, (G_{1^\perp})_3)^T = (0, \mathcal{A}_3 f_2, \mathcal{A}_2 f_3)^T & \text{on "}\rightarrow\text{"} \\ \boldsymbol{G_{2^\perp}} = ((G_{2^\perp})_1, 0, (G_{2^\perp})_3)^T = (\mathcal{A}_3 f_1, 0, \mathcal{A}_1 f_3)^T & \text{on "}\uparrow\text{"} \\ \boldsymbol{G_{3^\perp}} = ((G_{3^\perp})_1, (G_{3^\perp})_2, 0)^T = (\mathcal{A}_2 f_1, \mathcal{A}_1 f_2, 0)^T & \text{on "}\odot\text{"} \end{cases} \quad (2.28)$$

and $\mathcal{A}_\square$ (the adjoint of $\mathcal{A}_+$, see (3.6)) takes the normal component of transversal vectors

on the edges of a face onto the center of the face,

$$\boldsymbol{\mathcal{A}}_\square : L^2(\bar{\Omega}_E; E^\perp) \mapsto L^2(\bar{\Omega}_F)$$

$$\boldsymbol{\mathcal{A}}_\square \boldsymbol{G} = \boldsymbol{f} = \begin{cases} f_1 = \mathcal{A}_2(G_{3\perp})_1 + \mathcal{A}_3(G_{2\perp})_1 & \text{on "}\Rightarrow\text{"} \\ f_2 = \mathcal{A}_3(G_{1\perp})_2 + \mathcal{A}_1(G_{3\perp})_2 & \text{on "}\Uparrow\text{"} \\ f_3 = \mathcal{A}_1(G_{2\perp})_3 + \mathcal{A}_2(G_{1\perp})_3 & \text{on "}\odot\text{".} \end{cases} \tag{2.29}$$

In (2.24), we have implicitly identified

$$\boldsymbol{\omega} = \begin{cases} \omega_1 & \text{on "}\Rightarrow\text{"} \\ \omega_2 & \text{on "}\Uparrow\text{"} \\ \omega_3 & \text{on "}\odot\text{"} \end{cases}$$

with

$$\boldsymbol{\omega} = \begin{cases} (\omega_1, 0, 0)^T & \text{on "}\Rightarrow\text{"} \\ (0, \omega_2, 0)^T & \text{on "}\Uparrow\text{"} \\ (0, 0, \omega_3)^T & \text{on "}\odot\text{"} \end{cases}$$

so that $\boldsymbol{\omega}$ and $\boldsymbol{\mathcal{A}}_+\boldsymbol{u}$ are both vector fields defined on Ω_E, and $\boldsymbol{\omega} \times \boldsymbol{\mathcal{A}}_+\boldsymbol{u}$ is simply the usual cross product in $\mathbb{R}^3$. Furthermore, $\boldsymbol{\omega} \times \boldsymbol{\mathcal{A}}_+\boldsymbol{u} \in L^2(\bar{\Omega}_E; E^\perp)$ and is mapped to $L^2(\bar{\Omega}_F)$ by $\boldsymbol{\mathcal{A}}_\square$. $\boldsymbol{\mathcal{A}}_\square(\boldsymbol{j} \times \boldsymbol{\mathcal{A}}_+\boldsymbol{b})$ is defined in the same manner.

2.3. *The Fully Discrete Scheme*

With the notation introduced above, we proceed with the fully discrete MAC–Yee scheme with the dissipative terms and nonlinear terms treated explicitly using the forward Euler method as time discretization. The actual implementation is classical third- or fourth-order Runge–Kutta schemes for stability consideration as explained in [8]. The extension from forward Euler to RK3 or RK4 is straightforward:

$$\frac{\boldsymbol{u}^{n+1} - \boldsymbol{u}}{\Delta t} + \boldsymbol{\mathcal{A}}_\square(\boldsymbol{\omega} \times \boldsymbol{\mathcal{A}}_+\boldsymbol{u}) + \nabla_h p^{n+1} = -\nu\nabla_h \times \boldsymbol{\omega} + \alpha\boldsymbol{\mathcal{A}}_\square(\boldsymbol{j} \times \boldsymbol{\mathcal{A}}_+\boldsymbol{b}) \quad \text{on } \Omega_F \tag{2.30}$$

$$\nabla_h \cdot \boldsymbol{u}^{n+1} = 0 \quad \text{on } \Omega_C \tag{2.31}$$

$$\frac{\boldsymbol{b}^{n+1} - \boldsymbol{b}}{\Delta t} - \nabla_h \times \boldsymbol{\varepsilon} = -\eta\nabla_h \times \boldsymbol{j} \quad \text{on } \Omega_F. \tag{2.32}$$

Here variables without the superscript represent quantities at time step t^n.

In actual computations, we decompose the fluid part into several steps in the setting of projection method [5]: First we introduce an intermediate velocity variable $\boldsymbol{u}^* = (u_1^*, u_2^*, u_3^*)$:

$$\frac{\boldsymbol{u}^* - \boldsymbol{u}}{\Delta t} + \boldsymbol{\mathcal{A}}_\square(\boldsymbol{\omega} \times \boldsymbol{\mathcal{A}}_+\boldsymbol{u}) = -\nu\nabla_h \times \boldsymbol{\omega} + \alpha\boldsymbol{\mathcal{A}}_\square(\boldsymbol{j} \times \boldsymbol{\mathcal{A}}_+\boldsymbol{b}) \quad \text{on } \Omega_F. \tag{2.33}$$

The perfectly conducting wall condition and the no-slip condition can be easily realized numerically using local formulas:

$$j_\tau = 0 \quad \text{on } \Gamma_E, \tag{2.34}$$

$$u_\nu = 0 \quad \text{on } \Gamma_F, \tag{2.35}$$

$$\mathcal{A}_\nu(u_{\tau'}) = 0 \quad \text{on } \Gamma_E. \tag{2.36}$$

In this step, we can directly evaluate $\boldsymbol{u}^*$ at all the interior faces using (2.33) and impose

$$u_\nu^* = 0 \quad \text{on } \Gamma_F. \tag{2.37}$$

Second, we subtract (2.33) from (2.30) to get

$$\frac{\boldsymbol{u}^{n+1} - \boldsymbol{u}^*}{\Delta t} + \nabla_h p^{n+1} = 0 \quad \text{on } \Omega_F. \tag{2.38}$$

To recover p^{n+1}, we derive the pressure Poisson equation. Take $\nabla_h \cdot$ on (2.38) and apply (2.31),

$$\Delta_h p^{n+1} = \frac{1}{\Delta t} \nabla_h \cdot \boldsymbol{u}^* \quad \text{on } \Omega_C. \tag{2.39}$$

From (2.37), p^{n+1} naturally satisfies the Neumann boundary condition

$$\mathcal{D}_\nu p^{n+1} = 0 \quad \text{on } \Gamma_F. \tag{2.40}$$

Finally we update $\boldsymbol{u}^{n+1}$ from (2.38). The computation of $\boldsymbol{b}^{n+1}$ is straightforward from (2.32) and the boundary conditions (2.34)–(2.36).

In this setting, the divergence-free constraint for the magnetic field is satisfied automatically. Indeed, if we compute $\frac{1}{\Delta t}(\nabla_h \cdot \boldsymbol{b}^{n+1} - \nabla_h \cdot \boldsymbol{b}^n)$ on Ω_C using (2.32), we see exact cancellations among ε_l and j_l, $l = 1, 2, 3$, and therefore $\nabla_h \cdot \boldsymbol{b}^{n+1} = 0$, provided $\nabla_h \cdot \boldsymbol{b} = 0$ initially.

As shown in [8], the stability constraint for the transport diffusion operator

$$\partial_t + a\mathcal{D} - \nu\mathcal{D}^2$$

with centered differencing spatial discretization and third- or fourth-order Runge–Kutta time discretization is given by

$$\frac{a\,\Delta t}{\Delta x} \le C_1 \tag{2.41}$$

and

$$4\nu \frac{\Delta t}{\Delta x^2} \le C_2. \tag{2.42}$$

There is no cell Reynolds number constraint imposed by stability consideration. Thus the time stepping for (2.24)–(2.27) is governed by the CFL condition when $\max(\eta, \nu) \ll 1$.

In typical laboratory applications, the magnetic Reynolds number $1/\eta \le 0.5$. An explicit treatment for the resistive term imposes the parabolic time-stepping constraint in (2.42). In this case, we can switch to treat the resistive term of the Faraday equation implicitly:

$$\frac{\boldsymbol{b}^{n+1} - \boldsymbol{b}}{\Delta t} - \nabla_h \times \varepsilon = -\eta \nabla_h \times \boldsymbol{j}^{n+1} \quad \text{on } \Omega_F. \tag{2.43}$$

We can solve $\boldsymbol{b}^{n+1}$ efficiently as follows:

From (2.43), we have $\nabla_h \cdot \boldsymbol{b}^{n+1} = 0$. In view of (2.15), we can write (2.43) as

$$\frac{\boldsymbol{b}^{n+1} - \boldsymbol{b}}{\Delta t} - \nabla_h \times \varepsilon = \eta \Delta_h \boldsymbol{b}^{n+1} \quad \text{on } \Omega_F; \qquad (2.44)$$

thus the equations for b_i^{n+1}, $i = 1, 2, 3$, are decoupled. A standard Poisson solver can be used to solve for $\boldsymbol{b}^{n+1}$ with proper boundary conditions. Indeed, if we require (2.43) to hold on Γ_F, then (2.34)–(2.36) implies

$$\frac{b_\nu^{n+1} - b_\nu}{\Delta t} = 0 \quad \text{on } \Gamma_F. \qquad (2.45)$$

Equation (2.45) together with (2.34) (evaluated at t^{n+1}) provides a full set of mixed Dirichlet–Neumann boundary conditions for (2.44).

It is worth mentioning here that (2.45), which also holds in the explicit case, is consistent with the following calculus fact: for $\boldsymbol{e}(x) \in (H^1(\Omega))^3$, $\boldsymbol{e} \times \boldsymbol{\nu}|_\Gamma = 0$ implies $(\nabla \times \boldsymbol{e}) \cdot \boldsymbol{\nu}|_\Gamma = 0$ and $\frac{\partial}{\partial t}(\boldsymbol{b} \cdot \boldsymbol{\nu})|_\Gamma = 0$ as a consequence of the Faraday equation (2.18).

If instead the fluid Reynolds number is small, the viscosity term must be treated implicitly. As the treatment of resistive term, we rewrite (2.30) as

$$\frac{\boldsymbol{u}^{n+1} - \boldsymbol{u}}{\Delta t} + \mathcal{A}_\square(\boldsymbol{\omega} \times \mathcal{A}_+\boldsymbol{u}) + \nabla_h p^{n+1} = \nu \Delta_h \boldsymbol{u}^{n+1} + \alpha \mathcal{A}_\square(\boldsymbol{j} \times \mathcal{A}_+\boldsymbol{b}) \quad \text{on } \Omega_F. \quad (2.46)$$

In this case, standard fast Poisson solvers can be used to solve for the intermediate velocity,

$$\frac{\boldsymbol{u}^* - \boldsymbol{u}}{\Delta t} + \mathcal{A}_\square(\boldsymbol{\omega} \times \mathcal{A}_+\boldsymbol{u}) = \nu \Delta_h \boldsymbol{u}^* + \alpha \mathcal{A}_\square(\boldsymbol{j} \times \mathcal{A}_+\boldsymbol{b}) \quad \text{on } \Omega_F$$

$$u_\nu^* = 0 \quad \text{on } \Gamma_F, \quad \mathcal{A}_\nu(u_{\tau'}^*) = 0 \quad \text{on } \Gamma_E \qquad (2.47)$$

followed by the projection step

$$\frac{\boldsymbol{u}^{n+1} - \boldsymbol{u}^*}{\Delta t} + \nabla_h p^{n+1} = 0 \quad \text{on } \Omega_F$$

$$u_\nu^{n+1} = 0 \quad \text{on } \Gamma_F, \qquad (2.48)$$

which can be realized by solving the following pressure Poisson equation:

$$\Delta_h p^{n+1} = \frac{1}{\Delta t} \nabla_h \cdot \boldsymbol{u}^* \quad \text{on } \Omega_C$$

$$\mathcal{D}_\nu p^{n+1} = 0 \quad \text{on } \Gamma_F. \qquad (2.49)$$

This is the first-order projection method [5, 25].

3. THE ENERGY IDENTITY

The most distinguishing feature of the MAC–Yee scheme is, through proper averaging of the nonlinear terms as we described, no numerical dissipation was introduced since a discrete analogue of the energy identity (3.1) holds; see Theorem 1. This is particularly important for accuracy consideration in high-Reynolds-number flow computation.

Like most physical systems, (2.16)–(2.18) has a natural conserved quantity, namely, the total energy. We take the inner product of (2.16) with $\boldsymbol{u}$, (2.18) with $\alpha\boldsymbol{b}$, and sum them up. After integrating by parts, we get the energy identity

$$\frac{1}{2}\frac{d}{dt}\int_\Omega (|\boldsymbol{u}|^2 + \alpha|\boldsymbol{b}^2|) + \int_\Omega (\nu|\boldsymbol{\omega}|^2 + \alpha\eta|\boldsymbol{j}|^2) = 0, \tag{3.1}$$

where we have used the boundary conditions (1.2). We will show that our numerical scheme satisfies the same identity with spatial derivatives replaced by central differences. A direct consequence is the nonlinear stability of our scheme and hence the error estimate [20].

For simplicity of presentation, we take $\Delta x = \Delta y = \Delta z = h$. We define

$$\langle \boldsymbol{f}, \tilde{\boldsymbol{f}} \rangle_{\bar\Omega_F} = h^3 \left(\sum_{\Rightarrow}{}' f_1 \tilde{f}_1 + \sum_{\Uparrow}{}' f_2 \tilde{f}_2 + \sum_{\odot}{}' f_3 \tilde{f}_3 \right),$$

$$\langle \boldsymbol{g}, \tilde{\boldsymbol{g}} \rangle_{\bar\Omega_E} = h^3 \left(\sum_{\rightarrow}{}' g_1 \tilde{g}_1 + \sum_{\uparrow}{}' g_2 \tilde{g}_2 + \sum_{\odot}{}' g_3 \tilde{g}_3 \right),$$

$$\langle\langle \boldsymbol{G}, \tilde{\boldsymbol{G}} \rangle\rangle_{\bar\Omega_E} = h^3 \left(\sum_{\rightarrow}{}' \boldsymbol{G_{1\perp}} \cdot \tilde{\boldsymbol{G}}_{\boldsymbol{1\perp}} + \sum_{\uparrow}{}' \boldsymbol{G_{2\perp}} \cdot \tilde{\boldsymbol{G}}_{\boldsymbol{2\perp}} + \sum_{\odot}{}' \boldsymbol{G_{3\perp}} \cdot \tilde{\boldsymbol{G}}_{\boldsymbol{3\perp}} \right),$$

$$\langle q, \tilde{q} \rangle_{\bar\Omega_C} = h^3 \sum_{\bullet} q\,\tilde{q},$$

$$\|\boldsymbol{f}\|_{\bar\Omega_E} = \sqrt{\langle \boldsymbol{f}, \boldsymbol{f} \rangle_{\bar\Omega_E}},$$

$$\|\boldsymbol{g}\|_{\bar\Omega_F} = \sqrt{\langle \boldsymbol{g}, \boldsymbol{g} \rangle_{\bar\Omega_F}},$$

with

$$\sum_{\Rightarrow}{}' r = \sum_{i=0}^{N_1}{}' \sum_{j=1}^{N_2} \sum_{k=1}^{N_3} r_{i,j-\frac{1}{2},k-\frac{1}{2}},$$

$$\sum_{\Uparrow}{}' r = \sum_{i=1}^{N_1} \sum_{j=0}^{N_2}{}' \sum_{k=1}^{N_3} r_{i-\frac{1}{2},j,k-\frac{1}{2}},$$

$$\sum_{\odot}{}' r = \sum_{i=1}^{N_1} \sum_{j=1}^{N_2} \sum_{k=0}^{N_3}{}' r_{i-\frac{1}{2},j-\frac{1}{2},k},$$

$$\sum_{\rightarrow}{}' r = \sum_{i=1}^{N_1} \sum_{j=0}^{N_2} \sum_{k=0}^{N_3}{}' r_{i-\frac{1}{2},j,k},$$

$$\sum_{\uparrow}{}' r = \sum_{i=0}^{N_1}{}' \sum_{j=1}^{N_2} \sum_{k=0}^{N_3} r_{i,j-\frac{1}{2},k},$$

$$\sum_{\odot}{}' r = \sum_{i=0}^{N_1}{}' \sum_{j=0}^{N_2}{}' \sum_{k=1}^{N_3} r_{i,j,k-\frac{1}{2}},$$

$$\sum_{\bullet} r = \sum_{i=1}^{N_1} \sum_{j=1}^{N_2} \sum_{k=1}^{N_3} r_{i-\frac{1}{2},j-\frac{1}{2},k-\frac{1}{2}}.$$

Here we use the primed sum to denote proper weighting:

$$\sum_{l=0}^{N}{}' r_l = \frac{1}{2}r_0 + \sum_{l=1}^{N-1} r_l + \frac{1}{2}r_N.$$

$\langle \cdot, \cdot \rangle_{\Gamma_F}$, and $\langle \cdot, \cdot \rangle_{\Gamma_E}$ are similarly defined as summation over boundary faces and edges with proper weights,

$$\langle f, \tilde{f} \rangle_{\Gamma_F} = h^2 \left(\sum_{\Rightarrow \in \Gamma_F}{}' f\tilde{f} + \sum_{\Uparrow \in \Gamma_F}{}' f\tilde{f} + \sum_{\odot \in \Gamma_F}{}' f\tilde{f} \right),$$

$$\langle g, \tilde{g} \rangle_{\Gamma_E} = h^2 \left(\sum_{\rightarrow \in \Gamma_E}{}' g\tilde{g} + \sum_{\uparrow \in \Gamma_E}{}' g\tilde{g} + \sum_{\odot \in \Gamma_E}{}' g\tilde{g} \right),$$

where

$$\sum_{\Rightarrow \in \Gamma_F}{}' r = \sum_{i=0,N_1} \sum_{j=1}^{N_2} \sum_{k=1}^{N_3} r_{i,j-\frac{1}{2},k-\frac{1}{2}},$$

$$\sum_{\Uparrow \in \Gamma_F}{}' r = \sum_{i=1}^{N_1} \sum_{j=0,N_2} \sum_{k=1}^{N_3} r_{i-\frac{1}{2},j,k-\frac{1}{2}},$$

$$\sum_{\odot \in \Gamma_F}{}' r = \sum_{i=1}^{N_1} \sum_{j=1}^{N_2} \sum_{k=0,N_3} r_{i-\frac{1}{2},j-\frac{1}{2},k},$$

$$\sum_{\rightarrow \in \Gamma_E}{}' r = \sum_{i=1}^{N_1} \sum_{j=0,N_2} \sum_{k=0}^{N_3}{}' r_{i-\frac{1}{2},j,k} + \sum_{i=1}^{N_1} \sum_{j=0}^{N_2} \sum_{k=0,N_3} r_{i-\frac{1}{2},j,k},$$

$$\sum_{\uparrow \in \Gamma_E}{}' r = \sum_{i=0}^{N_1}{}' \sum_{j=1}^{N_2} \sum_{k=0,N_3} r_{i,j-\frac{1}{2},k} + \sum_{i=0,N_1} \sum_{j=1}^{N_2} \sum_{k=0}^{N_3}{}' r_{i,j-\frac{1}{2},k},$$

$$\sum_{\odot \in \Gamma_E}{}' r = \sum_{i=0,N_1} \sum_{j=0}^{N_2}{}' \sum_{k=1}^{N_3} r_{i,j,k-\frac{1}{2}} + \sum_{i=0}^{N_1}{}' \sum_{j=0,N_2} \sum_{k=1}^{N_3} r_{i,j,k-\frac{1}{2}}.$$

We have the following discrete version of vector identities:

LEMMA 1. *Let $f \in L^2(\bar{\bar{\Omega}}_F)$, $g \in L^2(\bar{\Omega}_E)$, $G \in L^2(\bar{\Omega}_E; E^\perp)$, and $q \in L^2(\bar{\bar{\Omega}}_C)$. The following identities hold,*

$$\langle f, \nabla_h q \rangle_{\bar{\bar{\Omega}}_F} = -\langle \nabla_h \cdot f, q \rangle_{\bar{\bar{\Omega}}_C} + \langle f_\nu, \mathcal{A}_\nu q \rangle_{\Gamma_F}, \tag{3.2}$$

$$\langle f, \nabla_h \times g \rangle_{\bar{\bar{\Omega}}_F} = \langle \nabla_h \times f, g \rangle_{\bar{\Omega}_E} + \langle \mathcal{A}_\nu f_{\tau'}, g_\tau \rangle_{\Gamma_E}, \tag{3.3}$$

$$\langle f, \mathcal{A}_\Box G \rangle_{\bar{\bar{\Omega}}_F} = \langle\langle \mathcal{A}_+ f, G \rangle\rangle_{\bar{\Omega}_E} - \frac{h}{4} \langle \mathcal{D}_\nu f_{\tau'}, (G_{\tau^\perp})_{\tau'} \rangle_{\Gamma_E}, \tag{3.4}$$

where $(G_{\tau^\perp})_{\tau'} = G_{\tau^\perp} \cdot \tau'$.

Equations (3.2)–(3.4) can be reduced to the following one-dimensional version of summation-by-part identity; the proof is elementary, so we omit it here.

PROPOSITION 1. *Let f be a scalar function defined on the cell centers of a one-dimensional domain with uniform grids, and g defined on the grids*:

$$f_{l-\frac{1}{2}} = f\left(x_{l-\frac{1}{2}}\right), \qquad g_l = g(x_l).$$

Defining

$$(\mathcal{D}f)_l = \frac{1}{h}\left(f\left(x_{l+\frac{1}{2}}\right) - f\left(x_{l-\frac{1}{2}}\right)\right), \qquad (\mathcal{D}g)_{l-\frac{1}{2}} = \frac{1}{h}(g(x_l) - g(x_{l-1})),$$

$$(\mathcal{A}f)_l = \frac{1}{2}\left(f\left(x_{l+\frac{1}{2}}\right) + f\left(x_{l-\frac{1}{2}}\right)\right), \qquad (\mathcal{A}g)_{l-\frac{1}{2}} = \frac{1}{2}(g(x_l) + g(x_{l-1})),$$

we have the following identities:

$$h\sum_{l=1}^{N} f_{l-\frac{1}{2}}(\mathcal{D}g)_{l-\frac{1}{2}} = -h\sum_{l=0}^{N}{}' g_l(\mathcal{D}f)_l + g_N(\mathcal{A}f)_N - g_0(\mathcal{A}f)_0 \qquad (3.5)$$

$$\sum_{l=1}^{N} f_{l-\frac{1}{2}}(\mathcal{A}g)_{l-\frac{1}{2}} = \sum_{l=0}^{N}{}' g_l(\mathcal{A}f)_l - \frac{h}{4}g_N(\mathcal{D}f)_N + \frac{h}{4}g_0(\mathcal{D}f)_0. \qquad (3.6)$$

Proof of Lemma 1.

$$h\sum_{\Rightarrow}{}' f_1(\mathcal{D}_1 q) = h\sum_{j=1}^{N_2}\sum_{k=1}^{N_3}\sum_{i=0}^{N_1}{}'(f_1(\mathcal{D}_1 q))_{i,j-\frac{1}{2},k-\frac{1}{2}}$$

$$= -h\sum_{j=1}^{N_2}\sum_{k=1}^{N_3}\sum_{i=1}^{N_1}((\mathcal{D}_1 f_1)q)_{i-\frac{1}{2},j-\frac{1}{2},k-\frac{1}{2}}$$

$$+ \sum_{j=1}^{N_2}\sum_{k=1}^{N_3}(f_1(\mathcal{A}_1 q))_{N_1,j-\frac{1}{2},k-\frac{1}{2}} - \sum_{j=1}^{N_2}\sum_{k=1}^{N_3}(f_1(\mathcal{A}_1 q))_{0,j-\frac{1}{2},k-\frac{1}{2}}$$

$$= -h\sum_{\bullet}(\mathcal{D}_1 f_1)q + \sum_{\Rightarrow\in\{i=N_1\}}(f_1(\mathcal{A}_1 q)) - \sum_{\Rightarrow\in\{i=0\}}(f_1(\mathcal{A}_1 q)),$$

where we have used (3.5) in the second equality. Similarly,

$$h\sum_{\Uparrow}{}' f_2(\mathcal{D}_2 q) = -h\sum_{\bullet}(\mathcal{D}_2 f_2)q + \sum_{\Uparrow\in\{j=N_2\}}(f_2(\mathcal{A}_2 q)) - \sum_{\Uparrow\in\{j=0\}}(f_2(\mathcal{A}_2 q)), \quad (3.7)$$

$$h\sum_{\odot}{}' f_3(\mathcal{D}_3 q) = -h\sum_{\bullet}(\mathcal{D}_3 f_3)q + \sum_{\odot\in\{k=N_3\}}(f_3(\mathcal{A}_3 q)) - \sum_{\odot\in\{k=0\}}(f_3(\mathcal{A}_3 q)), \quad (3.8)$$

and (3.2) follows. Equations (3.3) and (3.4) follow similarly from (3.5) and (3.6), respectively. We omit the details.

THEOREM 1. *Let $\boldsymbol{u}, \boldsymbol{b}$ be the solution of (2.24)–(2.27) with boundary conditions (2.34)–(2.36). Then*

$$\frac{1}{2}\left(\|\boldsymbol{u}(t)\|_{\Omega_F}^2 + \alpha\|\boldsymbol{b}(t)\|_{\Omega_F}^2\right) + \int_0^t \left(\nu\|\boldsymbol{\omega}(s)\|_{\Omega_E}^2 + \alpha\eta\|\boldsymbol{j}(s)\|_{\Omega_E}^2\right) ds$$

$$= \frac{1}{2}\left(\|\boldsymbol{u}(0)\|_{\Omega_F}^2 + \alpha\|\boldsymbol{b}(0)\|_{\Omega_F}^2\right). \qquad (3.9)$$

Proof. We take the inner product of $\boldsymbol{u}$ with Eq. (2.24), $\alpha\boldsymbol{b}$ with Eq. (2.26), and sum them up:

$$\langle \boldsymbol{u}, \partial_t \boldsymbol{u} \rangle_{\bar{\Omega}_F} + \langle \boldsymbol{u}, \mathcal{A}_\square(\boldsymbol{\omega} \times \mathcal{A}_+ \boldsymbol{u}) \rangle_{\bar{\Omega}_F} + \langle \boldsymbol{u}, \nabla_h p \rangle_{\bar{\Omega}_F} + \nu \langle \boldsymbol{u}, \nabla_h \times \boldsymbol{\omega} \rangle_{\bar{\Omega}_F}$$

$$- \alpha \langle \boldsymbol{u}, \mathcal{A}_\square(\boldsymbol{j} \times \mathcal{A}_+ \boldsymbol{b}) \rangle_{\bar{\Omega}_F} + \alpha \left(\langle \boldsymbol{b}, \partial_t \boldsymbol{b} \rangle_{\bar{\Omega}_F} - \langle \boldsymbol{b}, \nabla_h \times (\mathcal{A}_+ \boldsymbol{u} \times \mathcal{A}_+ \boldsymbol{b}) \rangle_{\bar{\Omega}_F} \right.$$

$$\left. + \eta \langle \boldsymbol{b}, \nabla_h \times \boldsymbol{j} \rangle_{\bar{\Omega}_F} \right) = 0.$$

From Lemma 1 and the boundary conditions (2.34)–(2.36),

$$\langle \boldsymbol{u}, \mathcal{A}_\square(\boldsymbol{\omega} \times \mathcal{A}_+ \boldsymbol{u}) \rangle_{\bar{\Omega}_F} = \langle\langle \mathcal{A}_+ \boldsymbol{u}, \boldsymbol{\omega} \times \mathcal{A}_+ \boldsymbol{u} \rangle\rangle_{\bar{\Omega}_E} = 0,$$

$$\langle \boldsymbol{u}, \nabla_h p \rangle_{\bar{\Omega}_F} = \langle \nabla_h \cdot \boldsymbol{u}, p \rangle_{\bar{\Omega}_C} = 0,$$

$$\langle \boldsymbol{u}, \nabla_h \times \boldsymbol{\omega} \rangle_{\bar{\Omega}_F} = \langle \boldsymbol{\omega}, \boldsymbol{\omega} \rangle_{\bar{\Omega}_E},$$

$$\langle \boldsymbol{u}, \mathcal{A}_\square(\boldsymbol{j} \times \mathcal{A}_+ \boldsymbol{b}) \rangle_{\bar{\Omega}_F} = \langle\langle \mathcal{A}_+ \boldsymbol{u}, \boldsymbol{j} \times \mathcal{A}_+ \boldsymbol{b} \rangle\rangle_{\bar{\Omega}_E},$$

$$\langle \boldsymbol{b}, \nabla_h \times (\mathcal{A}_+ \boldsymbol{u} \times \mathcal{A}_+ \boldsymbol{b}) \rangle_{\bar{\Omega}_F} = \langle \nabla_h \times \boldsymbol{b}, \mathcal{A}_+ \boldsymbol{u} \times \mathcal{A}_+ \boldsymbol{b} \rangle_{\bar{\Omega}_E}$$

$$= \langle \boldsymbol{j}, \mathcal{A}_+ \boldsymbol{u} \times \mathcal{A}_+ \boldsymbol{b} \rangle_{\bar{\Omega}_E}$$

$$= -\langle\langle \mathcal{A}_+ \boldsymbol{u}, \boldsymbol{j} \times \mathcal{A}_+ \boldsymbol{b} \rangle\rangle_{\bar{\Omega}_E},$$

and (3.9) follows after integrating in time.

In addition to energy conservation, there are two more quadratic invariants, namely, the cross helicity

$$\frac{d}{dt} \int_\Omega \boldsymbol{u} \cdot \boldsymbol{b} + (\eta + \nu) \int_\Omega \boldsymbol{j} \cdot \boldsymbol{\omega} + \int_\Gamma (p\boldsymbol{b} + \eta \boldsymbol{u} \times \boldsymbol{j} + \nu \boldsymbol{b} \times \boldsymbol{\omega}) \cdot \boldsymbol{\nu} = 0 \qquad (3.10)$$

and the magnetic helicity

$$\frac{d}{dt} \int_\Omega \boldsymbol{a} \cdot \boldsymbol{b} + 2\eta \int_\Omega \boldsymbol{j} \cdot \boldsymbol{b} + \int_\Gamma (V\boldsymbol{b} + \boldsymbol{e} \times \boldsymbol{b}) \cdot \boldsymbol{\nu} = 0, \qquad (3.11)$$

where $\boldsymbol{a}$ is the vector potential

$$\nabla \times \boldsymbol{a} = \boldsymbol{b}, \qquad (3.12)$$

and V the electric potential satisfying

$$\partial_t \boldsymbol{a} + \boldsymbol{e} + \nabla V = \boldsymbol{0}. \qquad (3.13)$$

A common choice of the gauge is

$$\nabla \cdot \partial_t \boldsymbol{a} = 0$$

$$-\Delta V(\cdot, t) = \nabla \cdot \boldsymbol{e}(\cdot, t) \qquad (3.14)$$

$$V(\cdot, t) = 0 \quad \text{on } \Gamma.$$

In view of (3.14) and the boundary condition (1.2), the helicity identities (3.11) and (3.10) reduce to

$$\frac{d}{dt} \int_\Omega \boldsymbol{u} \cdot \boldsymbol{b} + (\eta + \nu) \int_\Omega \boldsymbol{j} \cdot \boldsymbol{\omega} + \int_\Gamma p\boldsymbol{b} \cdot \boldsymbol{\nu} = 0 \qquad (3.15)$$

and

$$\frac{d}{dt} \int_{\Omega} \boldsymbol{a} \cdot \boldsymbol{b} + 2\eta \int_{\Omega} \boldsymbol{j} \cdot \boldsymbol{b} = 0. \tag{3.16}$$

From Lemma 1 and the discrete boundary conditions (2.34)–(2.36), it is straightforward to derive the following discrete version of (3.15):

$$\langle \boldsymbol{u}, \boldsymbol{b} \rangle_{\bar{\Omega}_F}(t) + \int_0^t (\langle \boldsymbol{\mathcal{A}}_\nu p, b_\nu \rangle_{\Gamma_F}(s) + (\nu + \mu)\langle \boldsymbol{j}, \boldsymbol{\omega} \rangle_{\bar{\Omega}_E}(s)) \, ds = \langle \boldsymbol{u}, \boldsymbol{b} \rangle_{\bar{\Omega}_F}(0). \tag{3.17}$$

However, there is no natural discrete analogue of (3.16) for our scheme since $\boldsymbol{a} \in L^2(\bar{\Omega}_E)$ and $\boldsymbol{b} \in L^2(\bar{\Omega}_F)$ are defined on different grid points. To analyze the effect of the MAC–Yee scheme on the magnetic helicity, we average $\boldsymbol{a}$ and $\boldsymbol{b}$ to cell centers

$$\boldsymbol{\mathcal{A}}_\boxplus \boldsymbol{b} \stackrel{\text{def}}{=} \frac{1}{2} \begin{pmatrix} b_1(x - \Delta x/2, y, z) + b_1(x + \Delta x/2, y, z) \\ b_2(x, y - \Delta y/2, z) + b_2(x, y + \Delta y/2, z) \\ b_3(x, y, z - \Delta z/2) + b_3(x, y, z + \Delta z/2) \end{pmatrix} \quad \text{on } \Omega_C$$

$$\boldsymbol{\mathcal{A}}_\boxtimes \boldsymbol{a} \stackrel{\text{def}}{=} \frac{1}{4} \begin{pmatrix} a_1(x, y - \Delta y/2, z - \Delta z/2) + a_1(x, y + \Delta y/2, z - \Delta z/2) \\ \quad + a_1(x, y - \Delta y/2, z + \Delta z/2) + a_1(x, y + \Delta y/2, z + \Delta z/2) \\ a_2(x - \Delta x/2, y, z - \Delta z/2) + a_2(x + \Delta x/2, y, z - \Delta z/2) \\ \quad + a_2(x - \Delta x/2, y, z + \Delta z/2) + a_2(x + \Delta x/2, y, z + \Delta z/2) \\ a_3(x - \Delta x/2, y - \Delta y/2, z) + a_3(x + \Delta x/2, y - \Delta z/2, z) \\ \quad + a_3(x - \Delta x/2, y + \Delta y/2, z) + a_3(x + \Delta x/2, y + \Delta y/2, z) \end{pmatrix} \quad \text{on } \Omega_C,$$

evaluate

$$\langle \boldsymbol{\mathcal{A}}_\boxtimes \boldsymbol{a}, \boldsymbol{\mathcal{A}}_\boxplus \boldsymbol{b} \rangle_{\bar{\Omega}_C} = h^3 \sum_{\bullet} \boldsymbol{\mathcal{A}}_\boxtimes \boldsymbol{a} \cdot \boldsymbol{\mathcal{A}}_\boxplus \boldsymbol{b}, \tag{3.18}$$

and then monitor the quantity

$$\mathcal{M}_3(t) = \langle \boldsymbol{\mathcal{A}}_\boxtimes \boldsymbol{a}, \boldsymbol{\mathcal{A}}_\boxplus \boldsymbol{b} \rangle_{\bar{\Omega}_C}(t) + 2\eta \int_0^t \langle \boldsymbol{\mathcal{A}}_\boxtimes \boldsymbol{j}, \boldsymbol{\mathcal{A}}_\boxplus \boldsymbol{b} \rangle_{\bar{\Omega}_C}(s) \, ds \tag{3.19}$$

in our calculation. We expect $\mathcal{M}_3(t) = \mathcal{M}_3(0) + O(h^2)$ and the results seems even better; see Section 5 for details.

It would be desirable to have a numerical scheme that preserves all three of these physical invariants numerically. In a forthcoming paper, we will consider flows with coordinate symmetry, such as pipe flow, axisymmetric flow, and flow on a sphere, the cases in which the flow is effectively two-dimensional. In these cases, we introduce a generalized stream function and vorticity-stream formulation for the Navier–Stokes and MHD equations. A class of energy and helicity (both the cross-helicity and the magnetic helicity in the case of MHD equation) preserving schemes is developed for these flows using a different technique; see [20] for details.

4. EQUIVALENT NUMERICAL FORMULATIONS

In this section, we list a few equivalent formulation of the MAC–Yee scheme and comment on their efficiency. As in Section 2.3, we only illustrate the schemes with forward Euler time discretization.

4.1. *3-D Scheme*

In the primitive formulation (2.30)–(2.32), an additional subroutine is needed to recover the vector potential a to monitor the discrete magnetic helicity (3.19). This requires three Poisson solvers each time a is recovered. In practice, if the numerical value of a is of interest at each time step, an alternative scheme based on discretizing (3.13) can be derived as follows:

Suppose we are given $b \in L^2(\bar{\Omega}_F)$ and $a \in L^2(\bar{\Omega}_E)$ with $\nabla_h \times a = b$ at time t^n. To recover inductively a^{n+1} such that

$$\nabla_h \times a^{n+1} = b^{n+1} \tag{4.20}$$

with b^{n+1} given by (2.32), we notice that

$$b^{n+1} = \nabla_h \times (a + \Delta t(\varepsilon - \eta \nabla_h \times b)); \tag{4.21}$$

therefore a^{n+1} is a solution to (4.20) if

$$\frac{a^{n+1} - a}{\Delta t} - \varepsilon = -\eta \nabla_h \times b. \tag{4.22}$$

In fact, if we denote all cell vertices in Ω by

$$\Omega_V = \{(i\,\Delta x,\, j\,\Delta y,\, k\Delta z) \mid i = 1, 2, \ldots, N_1 - 1,\ \ j = 1, 2, \ldots, N_2 - 1,$$
$$k = 1, 2, \ldots, N_3 - 1\}$$

and all cell vertices on Γ by Γ_V, the general solutions to (4.20) are then given by

$$\frac{a^{n+1} - a}{\Delta t} - \varepsilon + \nabla_h V = -\eta \nabla_h \times b, \tag{4.23}$$

with an arbitrary $V \in L^2(\bar{\Omega}_V)$. This is a direct consequence of the following discrete version of Green's formula.

PROPOSITION 2. *Let $g \in L^2(\bar{\Omega}_E)$ with*

$$\nabla_h \times g = 0 \quad on\ \bar{\Omega}_F.$$

Then

$$g = \nabla_h \theta,$$

where $\theta \in L^2(\bar{\Omega}_V)$ is given by the line integral of g along the cell edges.

The derivation from (4.22) or (4.23) with (4.20) to (2.32) is trivial.

Equation (4.22) is good for η small, and the computational cost is comparable to (2.32). In this case, the boundary condition (2.34) becomes

$$\frac{a_\tau^{n+1} - a_\tau}{\Delta t} = 0 \quad \text{on } \Gamma_E \tag{4.24}$$

since $\epsilon_\tau = j_\tau = 0$ on Γ_E.

When η is large, the resistive term must be treated implicitly:

$$\frac{\boldsymbol{a}^{n+1} - \boldsymbol{a}}{\Delta t} - \varepsilon + \nabla_h V = -\eta \nabla_h \times \boldsymbol{b}^{n+1} \quad \text{on } \Omega_E. \tag{4.25}$$

With a proper choice of the gauge V, (4.25) can be solved efficiently:

$$\Delta_h V = \nabla_h \cdot \varepsilon \quad \text{on } \Omega_V \tag{4.26}$$

$$V = 0 \quad \text{on } \Gamma_V. \tag{4.27}$$

As in the implicit treatment of the primitive formulation, (4.25) and (4.26) together imply $\nabla_h \cdot \boldsymbol{a}^{n+1} = 0$ provided $\nabla_h \cdot \boldsymbol{a} = 0$ initially. Therefore (4.25) is equivalent to

$$\frac{\boldsymbol{a}^{n+1} - \boldsymbol{a}}{\Delta t} - \varepsilon + \nabla_h V = \eta \Delta_h \boldsymbol{a}^{n+1} \quad \text{on } \Omega_E. \tag{4.28}$$

The boundary condition (4.27) for V is chosen so that (4.24) remains valid for convenience. In addition to (4.24), one more boundary condition for a_ν^{n+1} must be supplied on the ghost edges to solve $\boldsymbol{a}^{n+1}$ from (4.28). The correct boundary condition is

$$\nabla_h \cdot \boldsymbol{a}^{n+1} = 0 \quad \text{on } \Gamma_V, \tag{4.29}$$

which serves as a Neumann boundary condition for a_ν^{n+1} in view of (4.24).

Since

$$\Delta_h \nabla_h \cdot \boldsymbol{a}^{n+1} = 0 \quad \text{on } \Omega_V \tag{4.30}$$

from (4.28), (4.29) implies

$$\nabla_h \cdot \boldsymbol{a}^{n+1} = 0 \quad \text{on } \Omega_V.$$

A standard Poisson solver can be utilized to solve for a_i^{n+1}, $i = 1, 2, 3$, separately from (4.28), (4.24), and (4.29).

In summary, the implicit treatment for the resistive term at low magnetic Reynolds number, (4.28) and (4.26) with boundary conditions (4.24), (4.30), and (4.27) solves the Faraday equation in terms of the vector potential at the expense of one additional Poisson solver for each forward Euler time step, compared to the primitive formulation (2.44).

4.2. *2-D Scheme*

In this section, we derive an alternative formulation of the MAC–Yee scheme based on the discretization of the ω–a formulation of the 2-D MHD equation [2, 6]:

$$\partial_t \omega + \boldsymbol{u} \cdot \nabla \omega = \nu \Delta \omega + \alpha \boldsymbol{b} \cdot \nabla J$$
$$-\Delta \psi = \omega \tag{4.31}$$
$$\partial_t a + \boldsymbol{u} \cdot \nabla a = \eta \, \Delta a.$$

We show that proper treatment of the nonlinear terms and boundary conditions for (4.31) leads to a numerically equivalent formulation of the MAC–Yee scheme.

The 2-D MAC–Yee scheme (2.30)–(2.32) (see Fig. 3 for the 2-D version of grid notations) takes the form

$$\frac{u_1^{n+1} - u_1}{\Delta t} - \mathcal{A}_2(\omega \mathcal{A}_1 u_2) + \mathcal{D}_1 p = -\nu \mathcal{D}_2 \omega - \alpha \mathcal{A}_2(J \mathcal{A}_1 b_2) \quad \text{on ``}\Rightarrow\text{''},$$

$$\frac{u_2^{n+1} - u_2}{\Delta t} + \mathcal{A}_1(\omega \mathcal{A}_2 u_1) + \mathcal{D}_2 p = \nu \mathcal{D}_1 \omega + \alpha \mathcal{A}_1(J \mathcal{A}_2 b_1) \quad \text{on ``}\Uparrow\text{''},$$

$$\tag{4.32}$$

$$\mathcal{D}_1 u_1 + \mathcal{D}_2 u_2 = 0 \quad \text{on ``}\bullet\text{''}, \tag{4.33}$$

$$\frac{b_1^{n+1} - b_1}{\Delta t} - \mathcal{D}_2 \varepsilon = -\eta \, \mathcal{D}_2 J \quad \text{on ``}\Rightarrow\text{''},$$

$$\frac{b_2^{n+1} - b_2}{\Delta t} + \mathcal{D}_1 \varepsilon = \eta \, \mathcal{D}_1 J \quad \text{on ``}\Uparrow\text{''},$$

$$\tag{4.34}$$

with

$$\omega = \mathcal{D}_1 u_2 - \mathcal{D}_2 u_1,$$
$$J = \mathcal{D}_1 b_2 - \mathcal{D}_2 b_1 \qquad \text{on ``}\odot\text{''}, \tag{4.35}$$
$$\varepsilon = (\mathcal{A}_2 u_1)(\mathcal{A}_1 b_2) - (\mathcal{A}_1 u_2)(\mathcal{A}_2 b_1).$$

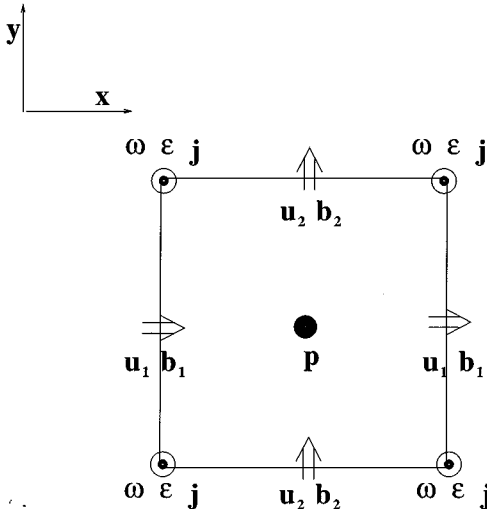**FIG. 3.** Mesh depiction for the 2-D MAC–Yee scheme.

Since $\nabla_h \cdot \boldsymbol{u} = \nabla_h \cdot \boldsymbol{b} = 0$, we can write

$$\boldsymbol{u} = \begin{pmatrix} \mathcal{D}_2 \psi \\ -\mathcal{D}_1 \psi \end{pmatrix}, \qquad \boldsymbol{b} = \begin{pmatrix} \mathcal{D}_2 a \\ -\mathcal{D}_1 a \end{pmatrix}, \tag{4.36}$$

with ψ and a defined on regular grids "$\odot$".

We now introduce the following notation:

$$\tilde{\mathcal{D}}_1 f(x, y) = \frac{f(x + \Delta x, y) - f(x - \Delta x, y)}{2\Delta x} \quad \text{on "$\odot$"} \tag{4.37}$$

$$\tilde{\mathcal{D}}_2 f(x, y) = \frac{f(x, y + \Delta y) - f(x, y - \Delta y)}{2\Delta y} \quad \text{on "$\odot$"} \tag{4.38}$$

$$\tilde{\nabla}_h \cdot \boldsymbol{f} = \tilde{\mathcal{D}}_1 f_1 + \tilde{\mathcal{D}}_2 f_2 \quad \text{on "$\odot$"} \tag{4.39}$$

and

$$\tilde{\boldsymbol{u}} = \begin{pmatrix} \tilde{u}_1 \\ \tilde{u}_2 \end{pmatrix} = \begin{pmatrix} \tilde{\mathcal{D}}_2 \psi \\ -\tilde{\mathcal{D}}_1 \psi \end{pmatrix}, \quad \tilde{\boldsymbol{b}} = \begin{pmatrix} \tilde{b}_1 \\ \tilde{b}_2 \end{pmatrix} = \begin{pmatrix} \tilde{\mathcal{D}}_2 a \\ -\tilde{\mathcal{D}}_1 a \end{pmatrix} \quad \text{on "$\odot$"}. \tag{4.40}$$

Since

$$\mathcal{A}_i \mathcal{D}_i = \mathcal{D}_i \mathcal{A}_i = \tilde{\mathcal{D}}_i,$$

we can write (4.32) and (4.34) as

$$\begin{aligned} \frac{u_1^{n+1} - u_1}{\Delta t} - \mathcal{A}_2(\omega \tilde{u}_2) + \mathcal{D}_1 p &= -\nu \mathcal{D}_2 \omega - \alpha \mathcal{A}_2(J \tilde{b}_2) \quad \text{on "$\Rightarrow$"} \\ \frac{u_2^{n+1} - u_2}{\Delta t} + \mathcal{A}_1(\omega \tilde{u}_1) + \mathcal{D}_2 p &= \nu \mathcal{D}_1 \omega + \alpha \mathcal{A}_1(J \tilde{b}_1) \quad \text{on "$\Uparrow$"} \end{aligned} \tag{4.41}$$

$$\begin{aligned} \frac{b_1^{n+1} - b_1}{\Delta t} - \mathcal{D}_2(\tilde{\boldsymbol{u}} \cdot \tilde{\nabla}_h a) &= -\eta \mathcal{D}_2 J \quad \text{on "$\Rightarrow$"} \\ \frac{b_2^{n+1} - b_2}{\Delta t} + \mathcal{D}_1(\tilde{\boldsymbol{u}} \cdot \tilde{\nabla}_h a) &= \eta \mathcal{D}_1 J \quad \text{on "$\Uparrow$"}. \end{aligned} \tag{4.42}$$

The Faraday equation can be formulated in terms of a as in the 3-D case,

$$\frac{a^{n+1} - a}{\Delta t} + \tilde{\boldsymbol{u}} \cdot \tilde{\nabla}_h a = \eta \Delta_h a \quad \text{on } \Omega_{\mathrm{V}} \tag{4.43}$$

$$\frac{a^{n+1} - a}{\Delta t} = 0 \quad \text{on } \Gamma_{\mathrm{V}}. \tag{4.44}$$

Here Ω_{V} and Γ_{V} refer to the regular grids, "$\odot$" points in Ω and Γ, respectively. The implicit treatment of the resistive term in (4.43) poses no difficulty and there is no need to introduce the gauge function.

As for (4.41), we apply $\nabla_h \times$ to obtain the vorticity-stream formulation for the fluid part,

$$\frac{\omega^{n+1} - \omega}{\Delta t} + \tilde{\nabla}_h \cdot (\omega \tilde{\boldsymbol{u}}) = \nu \Delta_h \omega + \alpha \tilde{\nabla}_h \cdot (J \tilde{\boldsymbol{b}}) \quad \text{on } \Omega_{\mathrm{V}}, \tag{4.45}$$

with the kinematic relation

$$\Delta_h \psi = -\omega \quad \text{on } \Omega_V. \tag{4.46}$$

The boundary conditions (2.35) and (2.36) read

$$\psi = 0 \quad \text{on } \Gamma_V, \tag{4.47}$$

and, say on $j = 0$,

$$\omega_{i,0} = \frac{2\psi_{i,1}}{\Delta x^2}, \tag{4.48}$$

which is known as Thom's formula.

The implicit treatment of the viscous term involves solving a biharmonic function and is usually quite expensive; we should go back to the primitive formulation (4.32)–(4.33) when ν is large.

The resulting ω–a formulation of the MAC–Yee scheme,

$$\partial_t \omega + \tilde{\nabla}_h \cdot (\omega \tilde{\boldsymbol{u}}) = \nu \Delta_h \omega + \alpha \tilde{\nabla}_h \cdot (\tilde{J}\boldsymbol{b})$$
$$\partial_t a + \tilde{\boldsymbol{u}} \cdot \tilde{\nabla}_h a = \eta \, \Delta_h a, \tag{4.49}$$

has significant saving in terms of memory and work over the original formulation in primitive variables (4.32)–(4.35).

In two-dimensional MHD equation, the magnetic helicity is identically zero and $\int_\Omega a^2$ emerges as an additional conserved quantity, taking place of the magnetic helicity:

$$\frac{d}{dt} \frac{1}{2} \int_\Omega a^2 + \eta \int_\Omega |\boldsymbol{b}|^2 - \eta \int_\Omega a \partial_\nu a = 0. \tag{4.50}$$

The discrete 2-D magnetic helicity

$$\mathcal{M}_2(t) = \frac{h^2}{2} \sum_{\tilde{\Omega}_V}{}' a(t)^2 + \eta \int_0^t h^2 \sum_{\tilde{\Omega}_V}{}' |\tilde{\boldsymbol{b}}(s)|^2 \, ds - \eta \int_0^t h \sum_{\Gamma_V}{}' (a \tilde{\mathcal{D}}_\nu a)(s) \, ds \tag{4.51}$$

is also monitored in our 2-D calculations. The primed sums in (4.51) denote properly weighted sums.

5. NUMERICAL RESULTS

We can show that the Mac–Yee scheme is second-order accurate for smooth solutions, based on the energy identity (3.9). The detail proofs will be presented elsewhere [20]. Here we give a few numerical examples to demonstrate the performance of the scheme. The time integrals in (3.9), (3.17), (3.19), and (4.51) were calculated using Simpson's formula. In all our examples, the discrete divergence of the calculated velocity and magnetic field, as well as the errors in the discrete energy identitiy (3.9) and cross-helicity identity (3.17) is within accumulation of roundoff errors, typically 10–12 digits accurate.

5.1. *Example 1*

Our first example is the 2-D Taylor vortex. This is a simple example used to demonstrate that the numerical solution has the right amount of viscosity. We take

$$\psi(x, y) = \sin(2\pi x)\sin(2\pi y)$$
$$a(x, y) = \sin(2\pi x)\sin(2\pi y)$$

as initial data with periodic boundary condition on $[0, 1]^2$. The exact solution is given by

$$\psi(x, y, t) = \sin(2\pi x)\sin(2\pi y)\exp(-8\pi^2\nu t)$$
$$a(x, y, t) = \sin(2\pi x)\sin(2\pi y)\exp(-8\pi^2\eta t).$$

In our test, we chose $\alpha = 1$, $\nu = 0.0001$, and $\eta = 0.02$. The exact solution has two distinct decay rates for ψ and a, respectively. The result at $t = 0.5$ with $\Delta t = 0.001$ is summarized in Table I. We see that the scheme is able to resolve the two rates correctly. In this particular example, (3.19) is accurate up to 12 digits because of the symmetry of the solution.

5.2. *Example 2*

Next, We take the forced flow in a confined box $\Omega = [0, 1]^3$ to check the accuracy of our 3-D code. We take $\alpha = 1$, $\nu = \eta = 0.001$, and

$$\boldsymbol{u}(x, y, z, t) = \cos(t)\begin{pmatrix} \sin^2(\pi x)(\sin(2\pi y) - \sin(2\pi z)) \\ \sin^2(\pi y)(\sin(2\pi z) - \sin(2\pi x)) \\ \sin^2(\pi z)(\sin(2\pi x) - \sin(2\pi y)) \end{pmatrix} \tag{5.1}$$

$$\boldsymbol{b}(x, y, z, t) = \cos(t)\begin{pmatrix} \sin(\pi x)(\cos(\pi y) - \cos(\pi z)) \\ \sin(\pi y)(\cos(\pi z) - \cos(\pi x)) \\ \sin(\pi z)(\cos(\pi x) - \cos(\pi y)) \end{pmatrix} \tag{5.2}$$

as an exact solution, use it to generate the corresponding forcing term, and append it to the right-hand side of (2.30) and (2.32). The exact formula of this forcing term is quite complicated so we omit it here. It is straightforward to modify the boundary condition (2.36) for the slip velocity in (5.1). The result at time $t = 2.0$ with $\Delta t = 0.0025$ is summarized in Table II. Second-order accuracy is clearly verified.

TABLE I
Errors and Orders of Accuracy for Example 1

	Mesh	L^2 error	Order	L^∞ error	Order
ω	32^2	1.257E−01	—	2.514E−01	—
	64^2	3.145E−02	1.999	6.290E−02	1.999
	128^2	7.864E−03	2.000	1.573E−02	2.000
J	32^2	1.219E−02	—	2.438E−02	—
	64^2	3.034E−03	2.007	6.068E−03	2.006
	128^2	7.577E−04	2.002	1.515E−03	2.002

Note. Parameters: $t = 0.5$, $\alpha = 1$, $\nu = 0.0001$, $\eta = 0.02$, and $\Delta t = 0.001$.

TABLE II

Errors and Orders of Accuracy for Example 2

	Mesh	L^2 error	Order	L^∞ error	Order
u	16^3	2.342E−02	—	5.800E−02	—
	32^3	5.433E−03	2.108	1.245E−02	2.220
	64^3	1.338E−03	2.022	3.063E−03	2.023
b	16^3	2.507E−01	—	6.811E−01	—
	32^3	5.586E−02	2.166	1.442E−01	2.240
	64^3	1.362E−02	2.036	3.537E−02	2.027

Note. Parameters: $t = 2$, $\alpha = 1$, $\nu = 0.001$, $\eta = 0.001$, and $\Delta t = 0.0025$.

5.3. *Example 3*

Next, we take

$$\boldsymbol{u}_0(x, y, z) = \begin{pmatrix} -2\sin(2\pi y)(1 - \cos(2\pi x))\sin(4\pi z) \\ -\sin(2\pi x)(1 - \cos(2\pi y))\sin(2\pi z) \\ \sin(2\pi x)\sin(2\pi y)(\cos(2\pi z) - \cos(4\pi z)) \end{pmatrix} \tag{5.3}$$

$$\boldsymbol{b}_0(x, y, z) = \begin{pmatrix} \sin(\pi x)(\cos(\pi y) - \cos(\pi z)) \\ \sin(\pi y)(\cos(\pi z) - \cos(\pi x)) \\ \sin(\pi z)(\cos(\pi x) - \cos(\pi y)) \end{pmatrix} \tag{5.4}$$

as initial data with the boundary conditions (2.34)–(2.360) and the parameters $\alpha = 1$, $\nu = 0.001$, $\eta = 0$. The error in $\mathcal{M}_3$ at time $t = 0.5$ with $\Delta t = 0.001$ is shown in Table III.

5.4. *Example 4*

Our final example is the Orszag–Tang vortex for ideal MHD equation on $[0, 2\pi]^2$ with periodic boundary condition. The initial data

$$\psi(x, y, 0) = 2(\cos(x) - \sin(y))$$
$$a(x, y, 0) = 2\cos(x) - \cos(2y) \tag{5.5}$$

are a pair of two vortices of opposite sign, centered at $(\pi, \pi/2)$ and $(\pi, 3\pi/2)$, respectively. Because of symmetry of the flow, the current sheet forms at later time near the two vortices. In

TABLE III

Errors and Orders of Accuracy for Example 3

	Mesh	Error	Order
$\mathcal{M}_3$	16^3	2.022E−03	—
	32^3	3.815E−04	2.406
	64^3	5.880E−05	2.698

Note. Parameters: $t = 0.5$, $\alpha = 1$, $\nu = 0.001$, $\eta = 0$, and $\Delta t = 0.001$.
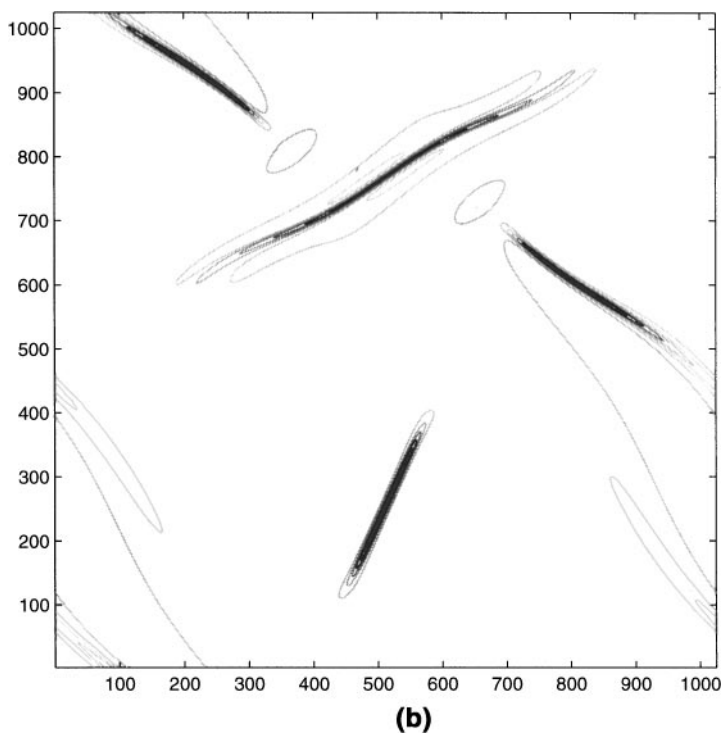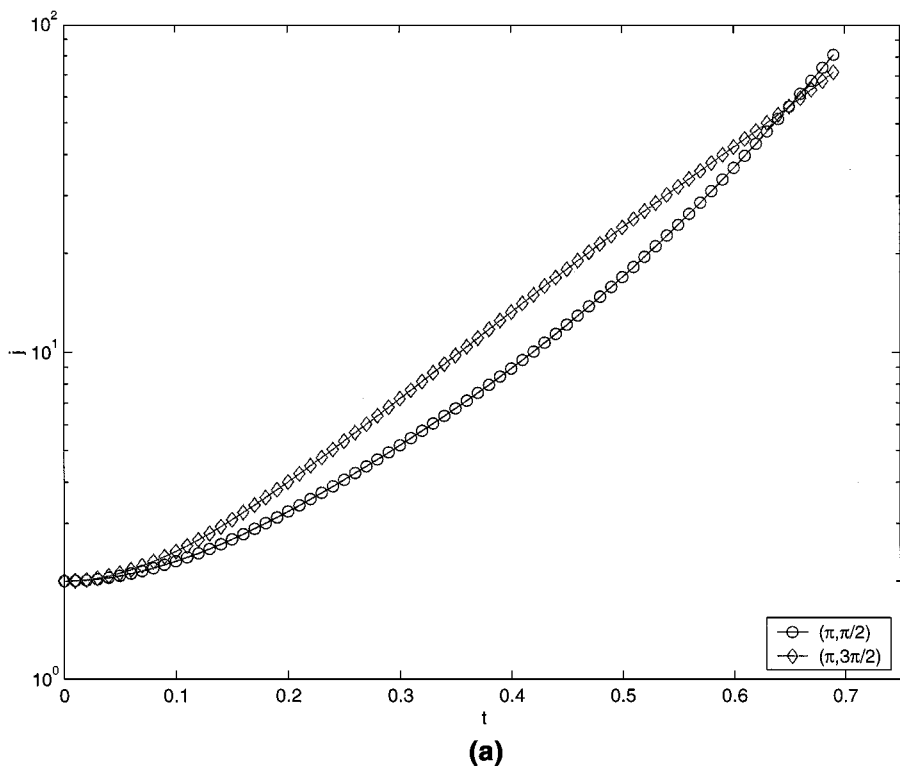
FIG. 4.   (a) Absolute value of the current density as a function of time at $(\pi, \pi/2)$ and $(\pi, 3\pi/2)$ in Example 4. (b) Contours of the current j at time $t = 0.75$ in Example 4 at 1024^2 resolution. (c) A closer look of (b) near the top current sheet. (d) Same as (c) with 512^2 resolution.
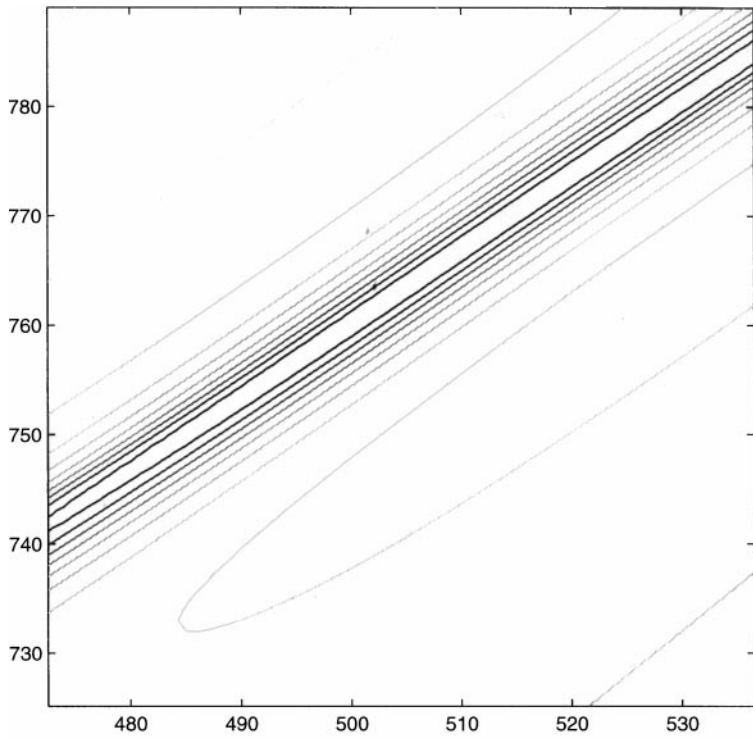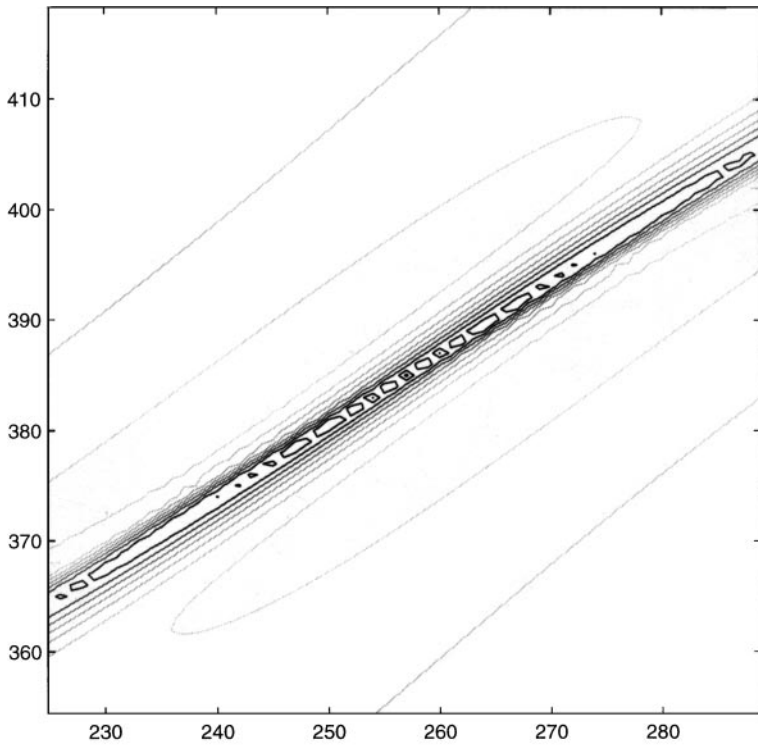
(c)

(d)

FIG. 4—*Continued*

TABLE IV
Errors and Orders of Accuracy for Example 4

	Mesh	Error	Order
$\mathcal{M}_2$	256^2	1.061E−03	—
	512^2	2.595E−04	2.032
	1024^2	6.440E−05	2.010

Note. Parameters: $t = 0.75$, $\alpha = 1$, $\nu = 0$, $\eta = 0$, and $\Delta t = 0.001$.

[6], a high-resolution scheme based on projection method with second-order upwinding and adaptive mesh refinement is used to simulate this problem. There a relative high resolution (equivalence of 32768^2 nonadaptive meshes) is used to calculate $\partial_x^2 a \partial_y^2 a - (\partial_x \partial_y a)^2$.

As a comparison, we repeat this calculation with 1024^2 grid points. It is clear from (2.41) and (2.42) that the MAC–Yee scheme can be applied to the ideal MHD under the CFL constraint. The time history of the local minimum of the current density at $(\pi, \pi/2)$ and $(\pi, 3\pi/2)$ is shown in Fig. 4a. The contour plot of 16 equally spaced level curves of the current density at $t = 0.75$ with $dt = 0.001$ is shown in Fig. 4b. Both of them agree well with the high-resolution calculation done in [6]. A blowup figure near $(\pi, 3\pi/2)$ (Fig. 4c) shows that the flow is well resolved with approximately 12 mesh size across the current sheet. The simplicity of this scheme and its remarkable performance lead us to believe that the MAC–Yee scheme is suitable for large time direct numerical simulation and probably the numerical search of possible singularity formation when combined with the local mesh refinement technique [1, 6]. This topic is currently under investigation.

At 512^2, the numerical solution starts to develop oscillations near the peaks of the current sheet because of lack of resolution (Fig. 4d). The result of the 256^2, 512^2, and 1024^2 runs shows that the discrete magnetic helicity (4.51) is second-order accurate (Table IV).

It is worth remarking here on the efficiency of the MAC–Yee scheme. Since the equation is completely decoupled with explicit treatment of the nonlinear terms and local boundary conditions, the scheme can make use of standard fast Poisson solvers such as FFT packages. Without specific optimization, the 64^3 calculation in Example 3 with double precision took about 20 s per time step on a laptop with a 266-MHz processor and 128 MB memory. The 1024^2 computation took about 30 s per time step on a PC with a 550-MHz processor and the job occupied about 145 MB of system memory.

ACKNOWLEDGMENTS

REFERENCES

1. M. J. Berger and P. Colella, Local adaptive mesh refinement for shock hydrodynamics, *J. Comput. Phys.* **82**, 64 (1989).

2. D. Biskamp, Collisional and collisionless magnetic reconnection, *Phys. Plasmas* **4**(5), 1964 (1997).

3. J. U. Brackbill and D. C. Barnes, The effect of nonzero $\nabla \cdot \mathbf{B}$ on the numerical solution of the magnetohydrodynamic equation, *J. Comput. Phys.* **35**, 426 (1980).

4. R. Caflisch, I. Klapper, and G. Steele, Remarks on singularities, dimension and energy dissipation for idea hydrodynamics and MHD, *Commun. Math. Phys*. **184**, 443 (1997).

5. A. J. Chorin, Numerical solution of the Navier–Stokes equations, *Math. Comput*. **22**, 745 (1968).

6. D. Cordoba and C. Marliani, Evolution of current sheets and regularity of ideal incompressible magnetic fluids in 2D, *Commun. Pure Appl. Math*. **53**, 512 (2000).

7. G. Duvaut and J. L. Lions, Inéqualions en thermoélasticité et magnétohydrodynamique, *Arch. Ration. Mech. Anal*. **46**, 241 (1972).

8. W. E. and J.-G. Liu, Vorticity boundary condition and related issues for finite difference schemes, *J. Comput. Phys*. **124**, 368 (1996).

9. R. Grauer and C. Marliani, Geometry of singular structures in magnetohydrodynamics flows, *Phys. Plasmas* **5**, 2544 (1998).

10. R. Grauer and C. Marliani, Current-sheet formation in 3D ideal incompressible magnetohydrodynamics, *Phys. Rev. Lett*. **84**, 4850 (2000).

11. M. Gunzburger and R. A. Nicolaides, *Incompressible Computational Fluid Dynamics* (Cambridge Univ. Press, Cambridge, 1993).

12. F. H. Harlow and J. E. Welch, Numerical calculation of time-dependent viscous incompressible flow of fluid with free surface, *Phys. Fluids* **8**, 2128 (1965).

13. C. He and Z. Xin, On the regularity of Solutions to Magnetohydrodynamics Equations, preprint.

14. C. He and Z. Xin, Partial Regularity of Suitable Weak Solutions to the Incompressible Magnetohydrodynamics Equations, preprint.

15. J. M. Hyman and M. Shashkov, Mimetic discretizations for maxwell's equations, *J. Comput. Phys*. **151**, 881 (1999).

16. J. M. Hyman and M. Shashkov, The orthogonal decomposition theorems for mimetic finite difference methods, *SIAM J. Numer. Anal*. **36**, 788(1998).

17. J. D. Jackson, *Classical Electrodynamics* (Wiley, NewYork, 1962).

18. R. M. Kerr and A. Brandenburg, Evidence for a singularity in ideal magnetohydrodynamics: Implication for fast reconnection, *Phys. Rev. Lett*. **83**, 1155 (1999).

19. I. Klapper, Constraints on finite-time current sheet formation at null points in two-dimensional ideal incompressible magnetohydrodynamics, *Phys. Plasmas* **5**, 910 (1998).

20. J.-G. Liu and W. C. Wang, Energy and helicity preserving finite difference schemes for flows with symmetry, preprint.

21. S. A. Orszag and C. Tang, Small-scale structure of two-dimensional magnetohydrodynamic turbulence, *J. Fluid Mech*. **90**, 129 (1979).

22. P. L. Sulem, U. Frisch, A. Pouquet, and M. Meneguzzi, On the exponential flattening of current sheets near neutral X-points in two-dimensional idea MHD flow, *J. Plasma Phys*. **33**, 191 (1985).

23. M. Sermange and R. Temam, Some mathematical questions related to the MHD equations, *Commun. Pure Appl. Math*. **36**, 635 (1983).

24. A Taflove, *Computational Electrodynamics: The Finite-Difference Time-Domain Method* (Artech House, Norwood, MA, 1995).

25. R. Temam, Sur l'approximation de la solution des equations de Navier–Stokes par la méthode des fractionnarires II, *Arch. Ration. Mech. Anal*. **33**, 377 (1969).

26. G. Tian and Z. Xin, One-point singular solutions to the Navier–Stokes equations, *Topol. Methods Nonlinear Anal*. **11**(1), 135 (1998).

27. T. C. Warburton and G. E. Karniadakis, A discontinuous Galerkin method for the viscous MHD equations, *J. Comput. Phys*. **152**, 608 (1999).

28. K. Yee, Numerical solution of initial boundary value problems involving Maxwell's equations in isotropic media, *IEEE Trans. Antennas and Propagation* **AP-16**, 302 (1966).